

Statistical Mechanics of Graphity Models

Tomasz Konopka

ITP, Utrecht University, Utrecht 3584 CE, the Netherlands

Graphity models are characterized by configuration spaces in which states correspond to graphs and Hamiltonians that depend on local properties of graphs such as the degrees of vertices and numbers of short cycles. As statistical systems, graphity models can be studied analytically by estimating their partition functions or numerically by Monte Carlo simulations. Results presented here are based on both of these approaches and give new information about the high- and low-temperature behavior of the models and the transitions between them. In particular, it is shown that matter degrees of freedom must play an important role in order for the low-temperature regime to be described by graphs resembling interesting extended geometries.

I. INTRODUCTION

The idea of describing space (or spacetime) as a product of a dynamical process involving some discretized elements resonates with many approaches to studying the unification of quantum mechanics with gravity [1, 2, 3, 4, 5, 6, 7, 8, 9, 10, 11, 12, 13, 14, 15, 16]. “Graphity” refers to a class of models in which the degrees of freedom represent dynamical graphs [17, 18] and whose Hamiltonians depend only on minimal information encoded in graphs such as the degree of the vertices and cycles formed by the edges. It has been argued that such models can be useful in studying how an extended and/or latticelike geometry might emerge from a background independent dynamical system.

Several approaches to studying quantum geometries are based on general or directed graphs and graphity models share some features with them while differing in others. In contrast to some setups defined primarily by a set of dynamical rules [4, 5, 6, 7], graphity models have Hamiltonians, which allow them to be interpreted as statistical mechanical systems. In contrast with approaches starting from a quantization ansatz for general relativity [8, 9, 10, 11, 12, 13], graphity models are only based on graph-theoretic notions and are not specific to a particular dimension or embedding manifold. They are in nature most similar to dynamical triangulations [8, 9, 10] in the sense that their macroscopic properties are determined by the collective interactions between a large number of small elements. The graph models are also amenable to simulation just like dynamical triangulations [8, 9, 10]. However, since not all general graphs correspond to triangulations, graphity models have a larger configuration space and their defining Hamiltonian cannot be easily mapped to a discretized version of the action of general relativity.

The motivation for studying such general systems comes from asking to what extent geometric notions such as the continuum, dimension, or macroscopic locality, should be considered as fundamental (as they are in all approaches that postulate the existence of a space or space-time manifold) and to what extent they may be only approximate or emergent. One way of probing these issues is to consider a setup in which none of these notions is obviously true. Graphity models are an attempt in this direction that assume only the existence of a Hamiltonian function

H determined by micro-local conditions of graphs (for a discussion of the distinction between macro and micro locality, see [19].)

It has been argued that graphity models can behave very differently at high and low energies [17, 18]. At low energies, the preferred graph state can represent an emergent geometry, while at high energies, the system is expected to be disordered and highly connected. The purpose of this paper is to study the statistical mechanics of the models in order to learn more about the nature of the low-temperature regime. The main finding is that while the most simple models do generate extended graphs at low temperatures, these graphs are effectively only one dimensional. However, when matter degrees of freedom that are sensitive to graph boundary conditions are added, the low-energy behavior can dramatically change and various homogenous latticelike graphs may appear. It thus appears that matter, as has been noticed in other contexts as well [16, 20, 21, 22], should be regarded as an important, if not crucial, factor in discussions of emergent geometries.

The definition of graphity models is reviewed in the next section. A distinction is made between a basic, or bare-bones, model of pure graphs and more sophisticated versions that can incorporate matter degrees of freedom in the form of gauge fields as well. The interpretation of the models as statistical systems is also introduced laying the ground for much of the following discussion. Section III deals with the partition function of the basic model. This discussion is detailed and involves identifying the types of graphs that can contribute significantly to the system's partition function. The discussion should be seen as complementary to the results of Monte Carlo simulations presented in Sec. IV. Indeed, it is the simulations that motivate and at the same time justify the study of particular types and the omission of other types of graphs in the theoretical section. As such, the analysis in Sec. III is an attempt to provide analytical understanding of the results of the numerical simulations. And in turn the analytical work suggests what kind of numerical studies can be of potential interest.

The results of the Monte Carlo simulations in Sec. IV indicate that the basic graphity model is insufficient to generate extended geometries with dimension greater than one in the low-energy regime. The emerging graphs are either chainlike or treelike. It is shown in this section, however, that supplementing the basic model with a condition for graph homogeneity does lead to very different and interesting results. This observation motivates the study of graph models with matter in Sec. V. The discussion there mirrors that in Sec. III and demonstrates that under certain quite general assumptions regarding the energy spectrum of the matter content, a model with a realistic matter component may indeed produce extended geometries at low temperature. A summary of all the findings is presented in Sec. VI.

II. GRAPHITY MODELS

Graphity [17, 18] is a name for a class of models in which states are associated with graphs and the configuration space is the space of all possible simple graphs with a given number of nodes N . The models are defined in a quantum mechanical context so that the configuration space is actually a Hilbert space. Indeed the Hamiltonian of the model is most naturally formulated as a quantum mechanical operator rather than as a classical object. For this reason, the models can also be referred to as “quantum” graphity.

The total Hilbert space for a graphity model can be decomposed as

$$\mathcal{H}_{total} = \bigotimes_{N(N-1)/2} \mathcal{H}_{edge} \bigotimes_N \mathcal{H}_{vertex}. \quad (1)$$

The tensor products of \mathcal{H}_{vertex} and \mathcal{H}_{edge} corresponds to putting degrees of freedom on each vertex and every possible edge connecting the vertices. Specific graphity models are defined by particular choices for the \mathcal{H}_{vertex} and \mathcal{H}_{edge} , along with an appropriate Hamiltonian acting on the resulting \mathcal{H}_{total} .

A. Basic Model

In the basic model described in [18], the Hilbert space associated with the vertices is trivial and the Hilbert space associated with each edge is spanned by two vectors

$$\mathcal{H}_{edge} = \text{span}\{|0\rangle, |1\rangle\}. \quad (2)$$

The total Hilbert space is therefore

$$\mathcal{H}_{total} = \bigotimes_{N(N-1)/2} \mathcal{H}_{edge}. \quad (3)$$

Denoting states in each copy of \mathcal{H}_{edge} as $|n_{ab}\rangle$ with $n_{ab} = 0, 1$, the total Hilbert space can be said to be spanned by the product states

$$\mathcal{H}_{total} = \text{span}\{|n_{12}\rangle \otimes |n_{13}\rangle \otimes |n_{23}\rangle \otimes \dots\} \quad (4)$$

A general state in this space is a superposition of the basis states with complex coefficients.

Interpreting the states $|1\rangle$ and $|0\rangle$ as conveying whether or not, respectively, a link is present between the two vertices, each of the basis states (4) can be associated with a graph configuration or a graph diagram. Thus, the total Hilbert space (3) can be decomposed as

$$\mathcal{H}_{edges} = \bigoplus_G \mathcal{H}_G \quad (5)$$

where \mathcal{H}_G is a space spanned by a single basis state and corresponds to a single graph G . Because the vertices are labeled and are thus distinguishable, the tensor summation over \mathcal{H}_G can contain multiple graphs G that are isomorphic to each other.

As argued in [18], a Hermitian Hamiltonian H acting on \mathcal{H}_{total} can be used to associate an energy $E(G)$ with a graph states $|\psi_G\rangle$ through the relation

$$E(G) = \langle \psi_G | : H : | \psi_G \rangle. \quad (6)$$

The form of the Hamiltonian is restricted by requirements of general graph locality and can thus depend only on a few properties of the graph. The basic model described in [18] uses a Hamiltonian of the form

$$H = H_V + H_B + H_{int} \quad (7)$$

where H_V depends on the degree of vertices, H_B depends on the cycle structure of a graph, and H_{int} is an interaction term. Each of the terms in the Hamiltonian can be implemented using creation and annihilation operators acting on \mathcal{H}_{total} [18]. For the purposes of this paper, however, it is sufficient to describe only the effective properties of the energies E associated with these terms.

The valence term H_V assigns an energy to the graph according to

$$E_V = g_V \sum_a e^{p(v(a)-v_0)^2}. \quad (8)$$

Here g_V is a positive coupling constant, p is some positive real number, $v(a)$ is the degree of vertex a , and v_0 is positive integer that determines the preferred valence of each vertex in the graph.

The other term H_B is such that its contribution to the energy can be written as

$$E_B = \sum_a E_B(a) \quad (9)$$

with

$$E_B(a) = - \sum_{L=3}^{N(N-1)/2} g_B(L) P(a, L). \quad (10)$$

The last expression is a contribution that corresponds to a single vertex a and that depends on the number of cycles $P(a, L)$ of length L that pass through that vertex. A cycle is defined as a closed walk along the edges of a graph in which no edge is traversed more than once (see [18] for more details.) The lower and upper limits on the sum are a consequence of this particular definition of a cycle.

The effective coupling $g_B(L)$ associated with cycles of each length is

$$g_B(L) = g_B \frac{r^L}{L!} \quad (11)$$

with g_B and r some constants. The form of this effective coupling plays a very important role in the properties of graphity models. The interplay between the exponential in the numerator and the factorial in the denominator of (11) means that the effective coupling increases with L for small L but decreases very rapidly for large L . The rapid falloff implies that the energy E_B is primarily determined by the number of short cycles in a graph. The total energy (10) may be well approximated by restricting the summation over L to the range $0 < L < L_{max}$ as follows:

$$E_B(a) \simeq - \sum_{L=3}^{L_{max}} g_B(L) P(a, L). \quad (12)$$

The maximal cycle length L_{max} must be determined for each model depending on the given parameters v_0 and r and on what accuracy the energy is to be evaluated.

The turnover between increasing and decreasing $g_B(L)$ occurs at some length L_* determined by the parameter r . When the effective coupling $g_B(L)$ is multiplied by the number of cycles $P(a, L)$, which usually increases with L , the maximum value of the product occurs at another

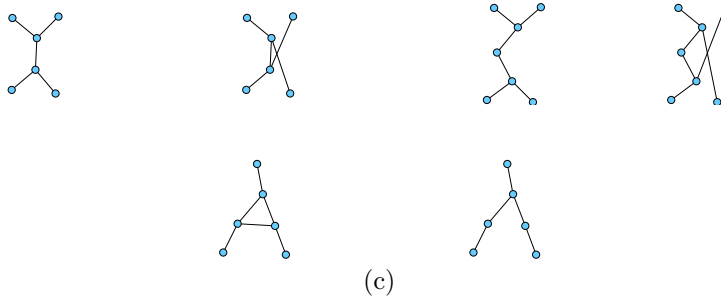


FIG. 1: Interaction moves on graphs.

length L_{**} determined by both r and the type of graph used to extract $P(a, L)$. Both scales L_* and L_{**} are smaller than L_{max} . It is important that none of these cycle length scales depend on the number of vertices in the graph N . Therefore, since only short cycles are important, the energy function can be said to be quasi-(micro)local.

Other important properties of (11) are determined by the signs of r and g_B . For $r > 0$ and $g_B > 0$, the effective coupling is positive definite; when it is inserted into the energy formula it is found that all cycles contribute a negative energy. When $r < 0$ and $g_B > 0$, the sign of $g_B(L)$ is different for even and odd cycles; even cycles contribute negative energy, and odd cycles contribute positive energy. Cases with $g_B < 0$ can be understood similarly.

Moving on from the definition of the cycle term, note that the basis states (4) are all eigenstates of the operators H_V and H_B . In order for the system to evolve from one graph configuration to another, an interaction term is necessary. While many forms of interactions acting on graph states are possible, the ones suggested in [17, 18] are among those that act locally on graphs. Examples of such interactions are shown in Fig. 1. The first two have the property that they preserve the degree of all vertices; the third move allows the degree to change. All of them preserve the connectedness of a graph state.

B. Model with Matter

Extensions of the basic model may involve introducing a nontrivial Hilbert space $\mathcal{H}_{vertices}$ for the vertices or extending the Hilbert space \mathcal{H}_{edge} associated with the edges. An example of the latter, described in [17, 18], consists of splitting the $|1\rangle$ state in the basic model into three distinct states so that

$$\mathcal{H}_{edge} = \text{span}\{|0\rangle, |1_1\rangle, |1_2\rangle, |1_3\rangle\}. \quad (13)$$

The states $|1_i\rangle$ denote “on” edges with different internal labels.

A Hamiltonian for the extended model can depend on the internal degrees of freedom of the on edges. Thus, in addition to analogs of the terms described in (7), other terms are also possible giving a total Hamiltonian of the form

$$H = H_V + H_B + H_{int} + H_M + H_G. \quad (14)$$

Here the notation H_M and H_G is meant to suggest that these terms may give rise to effective matter (H_M) and perhaps gravitational (H_G) dynamics. These terms could be implemented,

as originally suggested in [17, 18], using the string-net mechanism [23, 24, 25] related to the Kogut-Susskind formulation of gauge theory [26], or perhaps by other means, for example, by adapting the framework of algebraic quantum gravity to dynamical networks [13].

The specifics of the implementations of these terms will not be important for the work in the present paper. However, it might be expected that a realistic implementation should contain wavelike excitations such as photons or quantum mechanical particle wavefunctions in the matter spectrum. This rather weak assumption will be invoked in Sec. V.

C. Statistical Interpretation

As a statistical system, a graphity model can be studied by computing its partition function in the canonical ensemble at a characteristic temperature T . As the configurations of the basic graphity model correspond to graphs, the partition function can be written as

$$Z = \sum_G e^{-\beta E(G)}, \quad (15)$$

where $\beta = 1/k_B T$ is the inverse temperature, k_B is the Boltzmann constant, and $E(G)$ is the graph energy computed using (6).

In models containing extra degrees of freedom M , perhaps corresponding to matter, the partition function must involve another summation of those states,

$$Z = \sum_G \sum_M e^{-\beta E(G) - \beta E_M(G, M)}. \quad (16)$$

The energies E_M of the additional degrees of freedom can depend on the underlying graph configuration G , and so this dependence is explicitly shown in (16). When the main subject of study are graphs rather than the matter degrees of freedom, the summation over M can be hidden by writing

$$Z = \sum_G z(G) e^{-\beta E(G)} \quad (17)$$

with some function $z(G)$. It will be useful to note that both (15) and (17) can be cast into the general form

$$Z = \sum_G e^{-C(G)} \quad (18)$$

if the quantity $C(G)$ is defined as

$$C(G) = \beta E(G) - \ln z(G). \quad (19)$$

This quantity appearing in the exponent in the Boltzmann factor can be called the Boltzmann criterion. It reduces to the usual $\beta E(G)$ if the partition function for matter $z(G)$ is set to unity.

III. STATISTICAL MECHANICS OF THE BASIC MODEL

The purpose of this section is to estimate the partition function of a graphity model and use it to understand the statistical mechanics and “phase” structure of the model. Attention is restricted to classical graphity models so that the sum in the partition function is over the basis vectors of \mathcal{H}_{total} only, i.e. states that correspond to classical graphs. Furthermore, the matter factor is set to

$$z(G) = 1 \quad (20)$$

for simplicity, effectively putting the partition function in the basic form (15).

Since the aim of a graphity model is to describe an emergent geometry, emphasis is placed on understanding the partition function in the limit of a large number of vertices, $N \rightarrow \infty$. Since the models considered all have a finite number of vertices, this limit should be thought of in the following way. Consider a family of models each with a different N but with the same other basic parameters (couplings g_V , g_B or parameters v_0 , r). The equilibrium properties of each of these models can be evaluated separately. The continuum limit is understood as the limit of this series of systems arranged in order of increasing N .

The estimate for the partition function below is very crude and is based on only a few types of graphs. These are described in Sec. III A. It is argued that these few configurations are sufficient to extract basic information of the model such as the approximate transition temperatures. These properties, and the limit of applicability of the results, are described in Sec. III B.

A. Configurations

In any statistical system, some configurations have more importance than others in the partition function and thus in determining the expectation values of observables. In the context of graph models this means that some graphs, or classes of graphs, contribute more than others to Z . Understanding a graphity model can therefore be phrased as the problem of identifying the dominant classes of graphs and evaluating their contributions to Z .

In this section, it is argued that the important classes of graphs to consider are random graphs and graphs with lowest energy. Other types of graphs that are of interest and are also discussed are latticelike graphs. Thus, the partition function is split into

$$Z = Z_R + Z_L + Z_H + \dots \quad (21)$$

Each of these terms represents a sum like (15) restricted to a special class of graphs and will be estimated separately. The ellipsis denotes contributions from other graphs that do not fit into the mentioned categories.

In what follows the components of Z in (21) are written for large but finite N . This means that often only the dominant behavior of each term, as a function of N and β , is presented. Unless otherwise stated, estimates for $\ln Z$ are valid up to terms of order N , which can be neglected given that the dominant contributions are usually of order $N \ln N$. Dependence on the inverse temperature β is always shown explicitly even when it appears subleading as a function of N .

1. Low-Energy Graphs

A class of graphs that can contribute significantly to the partition function are those which have very small energy and thus a very large Boltzmann factor. Since the energy of a graph is determined by the valence and the cycle structure, minimizing the energy must take both of these properties into account. Consider regular graphs with varying degrees v . The number of cycles $P(a, L)$ of length L at each vertex a is bounded from above by

$$P(a, L) < c v^{L-1} \quad (22)$$

for some constant c . Since the bound is generous, the value of this constant is not important and can be set to unity. It follows that the total energy due to cycles is bounded by

$$\sum_a \sum_L g_B(L) P(a, L) < g_B N \frac{e^{|r|v}}{v}. \quad (23)$$

The absolute value in the exponent is required for the expression to hold for both negative and positive r . Putting this bound together with the energy contribution from vertex degrees, one obtains another bound $E_{0,v}$ for the total energy of regular graphs of degree v

$$E(G) > E_{0,v} = g_V N e^{p(v-v_0)^2} - g_B N \frac{e^{|r|v}}{v}. \quad (24)$$

The first term is minimum for $v = v_0$ and grows superexponentially for v different than v_0 . The magnitude of the second term increases with v but does so more slowly than the first term. Thus, it is possible to arrange the parameters so that the lowest possible energy occurs when the degree is v_0 . To do this, note that the energy of a v_0 -regular graph is smaller than

$$E_{v_0} = g_V N \quad (25)$$

and the energy of a $v_0 + 1$ -regular graph must be larger than

$$E_{v_0+1} = g_V N e^p - g_B N \frac{e^{|r|(v_0+1)}}{v_0 + 1}. \quad (26)$$

Setting $E_{v_0+1} - E_{v_0} > 0$ one finds

$$g_V (e^p - 1) - g_B \frac{e^{|r|(v_0+1)}}{v_0 + 1} > 0. \quad (27)$$

This is a conservative requirement on the couplings g_V and g_B that guarantees the lowest possible energy to be associated with a v_0 -regular graph (as opposed to a v -regular graph). When the inequality is satisfied, it also implies that the smallest energy graph is exactly regular – all graphs which break the regularity condition even at a select number of vertices have energy higher than the minimal energy regular graph. The condition also ensures that the energy function is bounded from below in the $N \rightarrow \infty$ limit.

In what follows, it will always be assumed that the couplings g_B and g_V are such that the minimal energy graph G_0 is v_0 -regular. The contribution of this graph to the partition function may be estimated as

$$Z_L \sim e^{N \ln N} e^{-\beta E(G_0)}. \quad (28)$$

It will be convenient to write this and all the following estimates in the form

$$\ln Z_L \sim N \ln N - \beta E(G_0). \quad (29)$$

Here, $E(G_0)$ is the minimum value of the energy associated to G_0 . The factor involving $N \ln N$ is due to the fact that there are on the order of $N!$ ways of assigning labels to the vertices of a graph with N vertices; although these different assignments are sometimes considered as equivalent from the graph-theoretic perspective, they correspond to distinct states in \mathcal{H}_{tot} and thus must be counted in Z_L .

The energy of a graph $E(G_0)$ can also be written as

$$E(G_0) = N(g_V + \epsilon_0) \quad (30)$$

giving ϵ_0 the interpretation as the average cycle energy per vertex in G_0 . Because of the form of the cycle term in the Hamiltonian, this quantity can be (and in cases of interest, is) negative. With this notation, Z_L becomes

$$\ln Z_L \sim N \ln N - \beta N (g_V + \epsilon_0). \quad (31)$$

There may be several other graphs G that have an energy $E(G)$ very close to $E(G_0)$. Such graphs could be interpreted as perturbations of G_0 and would contribute a quantity close to (31) to the full partition function. This could be taken into account by multiplying Z_L by the number of such perturbation graphs. However, this multiplicative factor should be expected to be on the order of N^x for some value x that does not strongly depend on N or β . Thus, for large N , the effect of such a multiplicative factor will be negligible compared with the other factors in (31) and hence will not be included in the analysis.

2. Random Graphs

Random graphs are configurations formed by randomly assigning edges to a set of vertices [27]. Regular random graphs are those random graphs that are subject to the constraint that all the vertices have equal degree. They are widely studied in graph theory, and a large number of their properties are known. For example, a typical random graph with a large number of vertices and low degree has almost no short cycles [27]. Thus, a typical random graph $G_{R,v}$ with degree v is assigned almost zero energy by the Hamiltonian H_B so that the total energy is entirely determined by the valence term

$$E(G_{R,v}) \sim g_V N e^{p(v-v_0)^2}. \quad (32)$$

Thus, compared to graphs with low energy discussed previously, the Boltzmann factor of random graphs can be small. However, because there are many random graphs in the space of all possible regular graphs, they may contribute significantly to the partition function overall.

The number of regular random graphs is difficult to evaluate for general v and N although some asymptotic formulae are known [27]. For the present purpose, an upper bound $W(N, v)$ for the number of random graphs will be sufficient. In a v -regular graph with N vertices, there are in total $N(N - 1)/2$ edges of which $Nv/2$ are “on.” The upper bound $W(N, v)$ may be estimated by the binomial coefficient

$$W(N, v) = \binom{Nv/2}{N(N - 1)/2} \quad (33)$$

This estimate overcounts graphs, because it does not take into account the requirement that the graph must be regular. When $N = 6$ and $v = 3$, for example, this estimate gives $W(6, 3) \sim 10^{14}$ whereas there are only two nonisomorphic three-regular graphs with six vertices, for a total of $2 \cdot 6! = 1440$ graphs. Nevertheless, the estimate becomes more accurate when N is large. In that regime, $W(N, v)$ can be expressed in a simpler form by writing out the binomial coefficient in terms of factorials and using the Stirling approximation. One finds

$$\ln W(N, v) \sim \frac{1}{2} Nv \ln N + O(N). \quad (34)$$

The random graphs that minimize (32) are those with $v = v_0$, and those will be of primary interest here. Thus, using the observation (32) and the upper bound (34), the estimate for the contribution to Z from v_0 -regular random graphs is

$$\begin{aligned} \ln Z_{R, v_0} &\sim \ln W(N, v_0) - \beta E(G_{R, v_0}) \\ &= \frac{1}{2} Nv_0 \ln N - \beta N g_V. \end{aligned} \quad (35)$$

Within the random graph category, there are also graphs which contain more than $Nv_0/2$ edges. These graphs necessarily have at least two vertices with degree different than v_0 . Such graphs have minimum energy if they can be thought of as consisting of a v_0 -regular random graph with an extra set of edges. The number of such graphs could be estimated by taking $W(N, v_0)$ and multiplying by N^{2x} , where x is the number of additional edges. For small x , the energy of such a graph would be different from $E(G_{r, v_0})$ by $xg_V(e^p - 1)$. Thus, the contribution to the partition function of such graphs would be written as

$$\ln Z_{R, v_0, x} \sim \ln Z_{R, v_0} + 2x \ln N - x\beta g_V(e^p - 1). \quad (36)$$

This formula can only be a reasonable estimate for small x . When x becomes comparable to N , some vertices would have degree greater than $v_0 + 1$, and the estimated energy shift used in (36) would break down. In fact, the energy penalty for those graphs would grow exponentially, and hence they would contribute negligibly to Z .

Summarizing the discussion on random graphs, their total contribution to Z is

$$Z_R = Z_{R, v_0} + \sum_x Z_{R, v_0, x} + \cdots \quad (37)$$

with x ranging from 1 to some number of order N and the ellipsis denoting further contributions from random graphs with more edges than $Nv_0/2 + x$. These contributions can be a priori very significant, but since the goal of the graphity model is to describe graphs with low degree, the discussion below in Sec. III B is devoted to finding conditions under which these contributions can be neglected. The terms shown in (37) will be sufficient for this purpose.

3. Homogeneous Graphs

Lattice graphs are graphs that are regular and further are highly homogeneous. Because of this, these graphs are of great interest from the perspective of using a graphity model to describe an emergent geometry. However, it is important to note that latticelike graphs may or may not correspond to graphs with lowest energy. As such, the contribution Z_H of homogeneous latticelike graphs should be considered separately from Z_L .

The estimated partition function Z_H may be written as

$$Z_H \sim \sum'_G e^{N \ln N} e^{-\beta N(g_V + \epsilon_H(G))}. \quad (38)$$

This has the same form as (31) but the additional sum is restricted (as denoted by the prime) to homogeneous, latticelike graphs G each of which has a cycle energy per vertex denoted by $\epsilon_H(G)$. The number of terms in the restricted sum that are large depends on parameters v_0 and r , but in general can be taken to be proportional to N or some power thereof. In comparison with the dependence on N of the individual terms, however, this scaling with N is insignificant. Furthermore, since the exponents in the Boltzmann factor of (38) are of the same form as in (31) but the energy per node ϵ_H is at most as small as ϵ_0 , the homogeneous graph contribution will in general be much smaller than Z_L for large N .

4. Other Graphs

The Hilbert space \mathcal{H}_{total} also supports a vast number of graphs that do not fit into the categories described above. Such graphs could be v_0 regular with some short cycles but not as many as G_0 , or almost regular with a few vertices breaking the valence condition, etc. They can be seen as configurations bridging the gaps between the random, low-energy, and homogeneous graphs.

Writing down a partition function for these graphs is as difficult as writing one down for the full model and will not be attempted here. However, in certain regimes the contribution of these intermediate graphs can be ignored. In situations where random graphs dominate the partition function, the intermediate graphs are subdominant because they are fewer in number. And in situations where low-energy graphs dominate, the intermediate graphs are also subdominant, because they have higher energy. In Sec. IV numerical simulations of the full system will provide a posteriori justification for ignoring these intermediate graphs.

B. Scaling and Thermodynamics

Given the arguments in Sec. III A, the partition function of a graphity model may be approximated by the contribution due to random graphs and low-energy graphs,

$$Z \simeq Z_R + Z_L. \quad (39)$$

Using (39), one can apply standard formulae

$$U = -\frac{\partial}{\partial\beta} \ln Z, \quad (40)$$

$$C = -\beta^2 \frac{\partial U}{\partial\beta} = \beta^2 \frac{\partial^2}{\partial\beta^2} \ln Z \quad (41)$$

to find the average energy U or the specific heat C . Since Z has a number of terms that may dominate in some temperature range, one can expect a number of maxima in the specific heat that correspond to transitions between the dominance regions of these terms. The canonical way of finding the temperatures of these transitions would be to consider $\partial C/\partial\beta = 0$ and solve for β . However, the resulting equations are very involved, and the solutions can only be written neatly after using some approximations. So, instead, one can treat the problem in a different manner.

Consider using only pairs of terms from (39) at a time to calculate the maxima in the specific heat. In particular, consider the pairs

$$Z_{L,v_0} = Z_L + Z_{R,v_0}, \quad (42a)$$

$$Z_{L,x} = Z_L + Z_{R,v_0,1}, \quad (42b)$$

$$Z_{v_0,x} = Z_{R,v_0} + Z_{R,v_0,1}. \quad (42c)$$

Each of these partition functions has only two terms. Thus, specific heats derived from them have one maximum each marking transitions between dominance regimes of the two terms. For example, the function Z_{L,v_0} has a characteristic inverse temperature that describes a transition from a v_0 -regular random graph regime (low β) to a low-energy graph regime (large β). As another example, the maximum in a specific heat derived from $Z_{v_0,x}$ describes a transition between graphs that should be expected to be v_0 -regular and graphs that have x extra edges.

In the limit $N \rightarrow \infty$, the maxima in the specific heats corresponding to (42) diverge. The transition inverse temperatures are given, in the large N limit, by

$$\beta_{L,v_0} = -\frac{1}{\epsilon_0} \left(\frac{v_0}{2} - 1 \right) \ln N \quad (43a)$$

$$\beta_{L,x} = -\frac{1}{\epsilon_0 - x\Delta\epsilon_V/N} \left(\frac{v}{2} - 1 + \frac{2x}{N} \right) \ln N \quad (43b)$$

$$\beta_{v_0,x} = \frac{2}{\Delta\epsilon_V} \ln N. \quad (43c)$$

In the latter two equations, the quantity

$$\Delta\epsilon_V = g_V (e^p - 1) \quad (44)$$

is always positive and can be made as large as desired by adjusting g_V . The quantity ϵ_0 , being the energy per vertex coming from the cycle term, is proportional to the coupling g_B , and in cases of interest is less than zero. At this stage, one can also note that the same transition temperatures could also be obtained by simply comparing the expressions for the components Z_L and Z_R without computing the specific heats and their maxima.

As all the expressions (43) contain a factor $\ln N$, the transitions they describe all technically occur at zero temperature in the $N \rightarrow \infty$ limit. This is perhaps not surprising as it can be already seen in expressions like (35) and (31) where the leading terms proportional to β are linear in N , while the leading terms independent of β scale as $N \ln N$. In the following, it is useful to either compare the solutions β at finite N , or to divide out by $\ln N$ to consider only the coefficients.

In order to reconstruct the transitions in the full system, one can compare the solutions (43) pairwise. Consider first the pair β_{L,v_0} and $\beta_{v_0,x}$. If the coupling condition (27) holds (as is necessary for the estimate Z_L to be consistent), then

$$\beta_{L,v_0} > \beta_{v_0,x}. \quad (45)$$

This implies that the lowest temperature regime is characterized by low-energy graphs and that there is a transition to exactly v_0 -regular random graphs at an inverse temperature β_{L,v_0} . The next transition at a much lower inverse temperature $\beta_{v_0,x}$ occurs between v_0 -regular random graphs and random graphs that are not-quite regular. An important thing to note is that these transitions can be well separated when g_V is large. Also, note that $\beta_{v_0,x}$ does not depend on x .

Next, consider the pair β_{L,v_0} and $\beta_{L,x}$. When x is order unity (as is assumed) and N is large, these two quantities become equal. It would be incorrect, however, to conclude that the transition from low-energy graphs to not-quite regular random graphs occurs at the same temperature as the transition to exact random graphs. This is because solution $\beta_{v,x}$ already implies that the transition to not-quite regular graphs occurs at much lower values of β . The apparent paradox is an artifact of using the simplified function $Z_{L,x}$, which does not take into account regular random graphs that form an intermediary stage between irregular graphs and low-energy graphs. The robust conclusion to draw from comparing β_{L,v_0} and $\beta_{L,x}$ is that low-energy graphs are stable at β higher than both of these values.

Comparing the final pair of solutions and observing that $\beta_{L,x} > \beta_{v_0,x}$ would suggest that graphs are v_0 -regular at the highest temperature, irregular at intermediary temperature, and low-energy at low temperature. While this is consistent with the hierarchy of the solutions (43), it is in conflict with the previous interpretation. Deciding between the two interpretations requires some extra input, and this can be obtained by calculating the expectation values of the energy around the transition $\beta_{v_0,x}$. It turns out that the original interpretation of the transitions with the irregular graphs as the highest energy stage is the correct one and, again, the apparent contradiction can be traced to the inappropriate use of the expression for $Z_{L,x}$.

The transition inverse temperatures (43) must be understood as only approximations to those one would find by considering the better approximation (39) or the full graphity partition function. Nonetheless, the property that the transition β s scale logarithmically with N should be consistent with what one would find from the full partition function. The estimate $\beta_{v_0,L}$ for the lowest temperature transition should also be accurate for large N (as will be confirmed in the next section). And furthermore, the separation of the transitions from low-energy graphs to regular random graphs and from regular random graphs to irregular graphs should also persist in the full model.

More specific questions regarding the nature of the transitions, however, cannot be addressed reliably. In particular, while (43) are all associated with diverging specific heats, the presented analysis does not make it clear whether these divergences persist in the full model and whether

they can actually be associated with phase transitions. One possibility is that the lowest-energy transition described by β_{L,v_0} is a true phase transition while the other transition $\beta_{v_0,x}$ is not. The first part of this expectation may be justified by the observation that phase transitions occur in other models in which there are vastly more high-energy states (random graphs) than low-energy states (low-energy graphs) [31]. However, like in other statistical models, the details may depend on the dimensionality of the graph in the low-energy regime. The second part of the expectation can be based on the fact that no such dramatic increase in the number of states is present among the regular and irregular random graphs. In addition to these uncertainties, it is also not known whether the quantum version of the model (one in which superpositions of classical graphs are allowed as quantum states) would exhibit the said phase transitions.

IV. SIMULATIONS

The main obstacle in evaluating the partition function of a graphity model is in enumerating the allowed graph configurations and in estimating their associated energies. Similar difficulties with other statistical systems have led to the development of various numerical approximation techniques. Notably among these are different types of Monte Carlo simulations [28]. Such techniques can also be used to address various questions relevant to a graphity model. For example, simulations can search for the lowest-energy graph for a given set of parameters N , v_0 , and r and couplings g_V and g_B . They can also provide estimates for the partition function and the expectation values of observables, such as the energy, for these parameters and couplings. This section describes results obtained through simulations of classical graphity models [29].

Given the expectation, justified in Sec. III, that states should be v_0 -regular at the lowest energies, all the simulations treat exactly v_0 -regular graphs only. This greatly simplifies the simulations and eliminates g_V from the list of parameters that can be explored. The coupling associated with cycles g_B , thus becomes the only coupling in the basic Hamiltonian and can thus be normalized to unity,

$$g_B = 1. \tag{46}$$

Despite the restriction to v_0 -regular graphs, the scope of the simulations must be further restricted for computational reasons. In particular, since counting cycles requires an algorithm that runs in exponential time in the length of the cycles, simulations are practically restricted to small values of L_{max} and thus of r .

The results presented were obtained using the Metropolis algorithm. The moves used to alter the graph during the simulation are those shown in Figs. 1(a) and Fig. 1(b), selected at random at each time step of the simulation. For a wide range of temperatures, the Metropolis algorithm performs well and produces results quickly. However, the graphity Hamiltonian does in principle produce an energy landscape that has multiple local minima, and hence the Metropolis algorithm encounters the danger of getting trapped in one of those local minima at very low temperature and not exploring the full configuration space. In this work, this problem is avoided mainly by using relatively small N , avoiding extremely large value of β , and repeating suspect simulations multiple times if needed. In some cases, the simulated tempering technique has also been tried, but all the results reported below rely only on the Metropolis method.

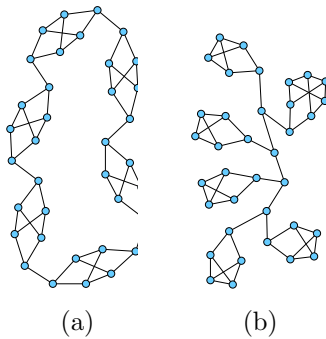


FIG. 2: Lowest-energy graphs in the basic model with $N = 36$ and with (a) $r = -2.5$ and (b) $r = 2.5$. The results are obtained through simulation at $\beta = 0.2$.

A. Basic Model

When studying the basic model only, the general graphity partition function (18) is restricted using

$$z(G) = 1, \quad C(G) = \beta E(G). \quad (47)$$

Within this framework, consider models defined by the parameters $v_0 = 3$ and $r = \pm 2.5$. The first parameter v_0 restricts the simulation to cubic graphs. The low value of the second parameter r suggests that only short cycles contribute significantly to the energy of a graph. However, since the Hamiltonian depends on cycles of various lengths, the length cutoff L_{max} must be set higher than the minimal cycle length. In practice, setting $L_{max} = 9$ allows to compute a graph's energy at the percent level.

1. Low-Energy Graphs

One set of simulations can be performed with the aim of finding the lowest-energy graph configuration. To do this, the initial state of the simulation should be sufficiently different from the expected minimal energy graph; random graphs make for good initial states and can be generated efficiently [30]. The simulation should further be performed with N and β suitably chosen so that the system evolves rather quickly toward low-energy states, while still allowing some fluctuations to occur. Fluctuations ensure that the true, rather than a local, energy minimum is found. After some trial and error, the values $N = 36$ and $\beta = 0.2$ are found to satisfy these criteria. The lowest-energy graphs found with these settings are shown in Fig. 2.

The two configurations shown are very distinct. When r is negative, the system effectively maximizes the number of 4-cycles in the graph. This leads to the graph in Fig. 2(a) containing six groups of six vertices connected in a chain. For positive r , the system allows some 3- and 5-cycles, and this results in the treelike structure shown in Fig. 2(b). Curiously, one of the leaves in Fig. 2(b) is different from all the others. This is because for $N = 36$ there can be no graph in which all the leaves have the most optimal five vertex structure. The position of the unique leaf on the tree is arbitrary, and thus the lowest-energy graph is degenerate.

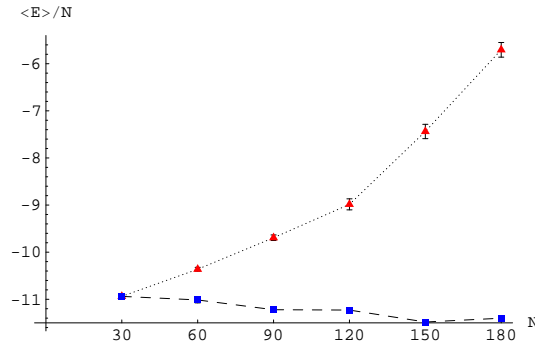


FIG. 3: Average energy per node as function of N in two series of simulations. Data points in the rising series are obtained through simulation with $v_0 =$, $r = -2.5$, and fixed $\beta = 0.17$. Data points in the flat series correspond to β scaling logarithmically with N . Error bars represent the standard error on the mean. The lines shown merely connect the data points and do not represent any fit.

The general features of Fig. 2 persist for other values of N , v_0 , and r . The lowest-energy states of systems with negative r are always chains of some small components. The internal structure and the size of these components depend on the particular choices of parameters, but the overall one-dimensional chainlike structure does not. For positive r , the lowest-energy structure is always a tree. Again, the structure of the leaves varies with r .

2. Scaling

The scaling estimates of Sec. III B suggest that systems should become increasingly dominated by random graphs in the large N limit unless the inverse temperature β scales at least logarithmically with N . This effect can be verified using Monte Carlo simulations.

Consider performing two series of simulations of the $r = -2.5$ model. In the first series, simulations at different N are performed always using $\beta = 0.17$. In the second series, the temperatures are chosen according to $\beta = \beta_0 \ln N$ with $\beta_0 = 0.17 / \ln 30$ so that the two series match for $N = 30$. In each simulation of each series, the expectation value (in the sense of the canonical ensemble) of the cycle energy per node, $\langle E(G) \rangle / N$, can be computed by extracting a number of representative configurations from the simulation and averaging them [28]. Since the lowest energy per node is independent of N for large N , this expectation value can be meaningfully compared across simulations with different N . The results are shown in Fig. 3.

In both series, the average energy per node is negative for $N = 30$. This indicates that the system is dominated by configurations close to the minimal energy state (the lowest possible energy per node for $r = -2.5$ is $\epsilon_0 = -12.2$). In the series with fixed β , however, $\langle E \rangle / N$ rises sharply with increasing N . This reveals a transition to a regime of the parameter space where random graphs start dominating over low-energy graphs. The line does not reach $\langle E \rangle / N \sim 0$, because for these still small values of N there are still a large number of graphs that have quite a large number of cycles but no longer resemble the chain structure. In other words, points with $\epsilon_0 < \langle E \rangle / N < 0$ represent graphs of the type omitted in the estimates of the partition

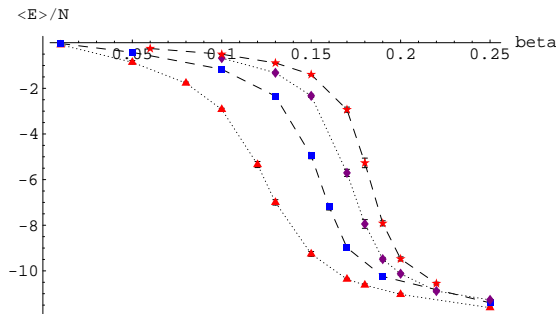


FIG. 4: Average energy per node for systems with $r = -2.5$ and N equal to (left to right) 60, 120, 180, and 240. Error bars on the points (some too small to be seen) represent the standard error on the mean. The lines do not represent computed data and are only shown to aid the eye distinguish between the four series.

function in Sec. III.

The second series shown in Fig. 3 is the one where β scales with N . In this case, the average energy per node remains very small even for large N indicating that the low-energy configurations continue to dominate. Note that the dip at $N = 150$, which seems to conflict with the slightly decreasing trend, is a statistical artifact - the point is actually within 2σ of the value corresponding to $N = 180$. However, the dip does indicate that the simulations start becoming less reliable at high N and increasing β because of the ruggedness of the energy landscape. This unreliability is a systematic error that is not included in the error bars shown on the plot.

The data in Fig. 3, as all numerical work, cannot prove the assertion that the required scaling of β must necessarily be logarithmic nor that the logarithmic scaling is sufficient for the average energy per node to remain close its minimum. This is particularly so because the explored range of N is small given that the expected dependence of the transition temperature on N is logarithmic. Nevertheless, the data show the Monte Carlo simulations of the full model to be consistent with the expected behavior derived in section III and thus provide an important consistency check for those estimates.

3. Transitions

Apart from verifying the estimated scaling of β , one can also study the low-energy to random graph transition in the standard manner by performing simulations at various β for fixed r and N . The results are shown in Figs. 4 and 5 for systems with $r = -2.5$ and $N = 60, 120, 180$, and 240.

The plot in Fig. 4 shows how the average cycle energy per node decreases as β increases. The transition is quite smooth for $N = 60$ but becomes sharper for larger N . This effect is mainly due to the fact that the difference in numbers of states in the low-energy and random regimes becomes more pronounced with large N . Also, random graphs with $N = 60$ might

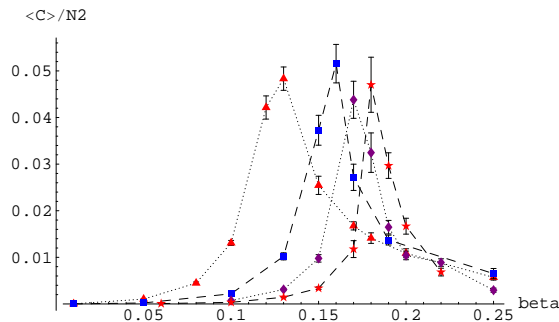


FIG. 5: Normalized specific heat for systems with $r = -2.5$ and N equal to (left to right) 60, 120, 180, and 240. Error bars are computed using the bootstrap resampling method. The lines do not represent computed data.

have quite a few short cycles thus lowering the average energy at low β . The location of the transition temperature shifts slightly to larger β with increasing N , which is consistent with the scaling of β found in Sec. III B.

Figure 5 shows the specific heat associated with the same simulations. The values plotted are actually specific heats divided by N^2 to make all four curves have roughly equal height. It should be noted that no special effort was made to find the true maxima of the specific heats. Doing that would require more computer time due to the “critical slowing down” phenomenon within the Monte Carlo simulation [28]. However, the location of these maxima can still be estimated from the plots: they occur roughly at $\beta = 0.13, 0.16, 0.17, 0.18$. These numbers can be compared with the estimates from Eq. (43a). Using $\epsilon_0 = -12.2$, one finds the expected transition inverse temperatures to be $\beta = 0.17, 0.20, 0.21$, and 0.22 . The estimates therefore consistently overshoot the real transition values by roughly 20%. While the agreement is not stunning, it does show that the estimate can be a useful guide for determining where the transition occurs.

B. Matter Using Variance

The general partition function of a graphity model, Eq. (17), includes a contribution $z(G)$ from the matter degrees of freedom. While the form of this matter factor must depend on how the matter is implemented in the model, it is reasonable to assume that this factor has some general features. It may be reasonable to assume, for example, that $z(G)$ is large for homogeneous graphs and small for graphs that contain many inhomogeneities. This observation suggests to study the effect of matter by choosing an ansatz for $z(G)$. A simple one is

$$\ln z(G) = -\mu V(G), \quad (48)$$

with μ a real number and

$$V(G) = \sum_a \left(E_B^2(a) - \frac{E_B^2}{N^2} \right) \quad (49)$$

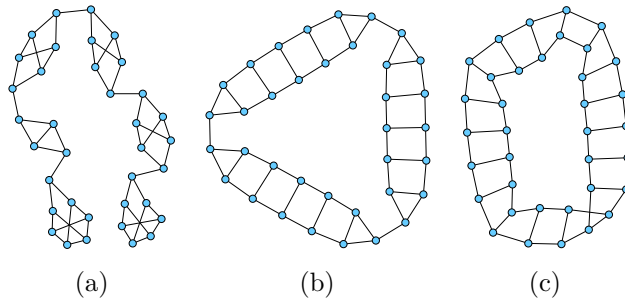


FIG. 6: Graphs with lowest criterion C for $N = 36$ and $r = +2.5$. Results are obtained with $\beta = 0.2$ and the variance potential set to (a) $\mu = 0.8$ (b) $\mu = 3$, and (c) $\mu = 4$.

the variance among the cycle energies $E_B(a)$ assigned to each vertex a in the graph G . This ansatz implies using the Boltzmann criterion $C(G)$ as

$$C(G) = \beta E(G) + \mu V(G). \quad (50)$$

Since μ now appears like a potential in statistical ensembles, it can be called the variance potential. When it is positive, inhomogeneous graphs are suppressed in the partition function.

The variance ansatz for $z(G)$ is not intended to mimic a particular type of matter. Rather, its main advantage is that it can be implemented in a straightforward fashion in Monte Carlo simulations. Searches for the lowest-criterion graph can now be conducted similarly as in Sec. IV A 1 for varying values of the variance potential μ .

1. Cubic Graphs

Consider augmenting the simulations from Sec. IV A 1 ($N = 36$, $v_0 = 3$, and $r = \pm 2.5$) by the matter ansatz with variance potential μ . The results for $r = +2.5$ are shown in Fig. 6. The graphs shown are more and more homogeneous for larger μ , and the ladder graph shown in Fig. 6(c) is entirely vertex-transitive. Interestingly, this graph contains no cycles of length three in sharp contrast to the ground state graph obtained when $\mu = 0$ shown in Figure 2(b). Simulations of the system with $r = -2.5$ with large μ yield the same ladder graph.

In terms of emergence of geometry, the results obtained show that an effective homogeneous one-dimensional space can be formed from the graphity model with $r = -2.5$. Moreover, for either sign of r but high enough μ , the emergent space can be the same.

Since the simulations leading to Fig. 6 are performed at low temperature, they can also give some indication as to what the next-to-lowest-energy graphs look like. Some of these graph excitations for the $r = -2.5$ simulation are shown in Fig. 7. These excitations quickly start looking like randomized graphs. Nonetheless, one can still recognize the background lowest-energy graph from their diagrams.

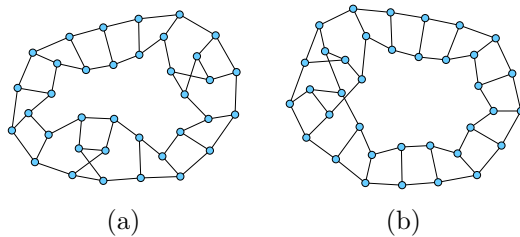


FIG. 7: Two graphs representing excitations of the $r = -2.5$ and high μ model.

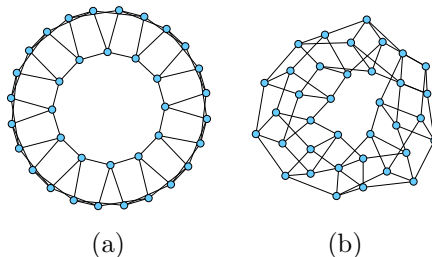


FIG. 8: Low-criterion quartic graphs. (a) is obtained with $r = -1.5$, $\beta = 0.6$ and $\mu = 32$. (b) is produced with $r = -2.5$, $\beta = 0.17$, and $\mu = 3.8$.

2. Quartic Graphs

Quartic graphs are graphs in which all vertices have degree four. Simulations with $v_0 = 4$ can be performed in the same manner as for cubic case. One new property of quartic graphs (and generally of regular graphs of degree larger than 3) is that long cycles may visit a given vertex more than once.

Quartic graphs are of interest because they can give rise to several types of latticelike configurations. In particular, the square lattice corresponds to flat 2D space and has four-sided plaquettes. Also, the diamond lattice corresponds to flat 3D space, and its shortest cycles have length six.

Simulations searching for graphs with lowest criterion $C(G)$ were performed for small values of r and large variance potential μ . Some of the results are shown in Fig. 8. Neither of the shown graphs is planar and this indicates that the emerging graphs might be interpreted as having dimension greater than one. Indeed both graphs in Fig. 8 may be thought of as two-dimensional tori. This is particularly convincing in the case of Fig. 8(b), where the two circumferences associated with a torus have lengths four and nine.

3. Graphs with Larger Plaquettes

Simulations with $|r|$ much greater than 2.5 encounter at least three problems. First, as $|r|$ increases, the evaluation of the graph energy becomes more time-consuming as longer cycles

must be taken into account. Second, in order to obtain results that can be generalized to the continuum limit, the number of vertices N used in the simulation must be large enough so that in the high- β regime, the energy per node of the emerging graph is not skewed by the finite value of N . And third, as $|r|$ increases, the depth of the valleys in the energy landscape increases. All three of these issues make it more difficult for a simple desktop simulation to provide accurate results quickly. More sophisticated methods like simulated tempering should likely be used to make real progress.

It is possible to perform some quick simulations with large $|r|$, for example $r = -6$, if L_{max} is set very small, for example $L_{max} = 7$. Such a low cutoff value for the cycle length means that the evaluation of the energy is not at all accurate. However, all three problems mentioned above become less serious. Simulations performed in this way with large β and large μ produce graphs with hexagonal plaquettes that resemble those graphs described in [18]. While this is encouraging in the sense that it suggests that interesting lattices may appear in other regions of the graphity parameter space, it should be stressed again that such simulations with low L_{max} cannot capture properties of the full graphity Hamiltonian. Proper simulations at large $|r|$ must thus be considered beyond the scope of this initial numerical exploration.

V. STATISTICAL MECHANICS OF A GRAPHITY MODEL WITH PARTICLES

In the previous section, the effect of matter on graph configurations was modeled by adding a term proportional to the vertex energy variance to the Boltzmann criterion. Simulations showed that large values of the variance potential can indeed change the type of graph that minimizes the Boltzmann criterion (19) and thus change the structure of the expected graph at low temperatures. But while the variance prescription is straightforward to implement in a Monte Carlo simulation, it does not fully incorporate the effect of matter on a graph. It does not, for example, account for the fact that spaces with different geometries may allow for different densities of particle states. Thus, it would be desirable to supplement, or replace, the variance prescription with something more realistic.

Since explicitly evaluating the partition function of a graphity model, with or without matter, is not feasible without approximations, one cannot, at least at this stage, learn very much by studying a particular form of matter coupling to graphs. This section therefore focusses on general properties of wavelike matter and discusses how they affect a dynamical geometry such as in a graphity model. The main principles leading to the argument that matter can significantly alter, and even determine, the shape of a dynamical geometry are outlined below in section V A. These principles are then applied to dynamical graphs in Secs. V B and V C. As in Sec. III, only the leading terms in N and β will be written in the estimates for the partition function components.

A. Flexible Boxes

Consider a set of N particles in a two-dimensional rectangular box with fixed area A in which the lengths L_x and L_y of the two sides can vary as long as $L_x L_y = A$. As the geometry of the box is not fixed, the partition function of the system includes a summation over the

configurations, denoted (L_x, L_y) , that the box can take. It can be written as

$$Z = \sum_{(L_x, L_y) \in \mathcal{C}} z(L_x, L_y) e^{-\beta E_B(L_x, L_y)} \quad (51)$$

where $E_B(L_x, L_y)$ is the energy associated with a given box, and $z(L_x, L_y)$ describes the matter content. In the case that $E_B(L_x, L_y) = 0$ for all L_x and L_y , the properties of the system, including its geometry, are determined by the matter factors and the space of configurations \mathcal{C} over which the sum is taken.

The space of configurations is the set \mathcal{C} of possible pairs of lengths (L_x, L_y) . For the present purpose, the precise form of this set will not be important, and only some of its general features will be assumed and used. First, the set \mathcal{C} should contain certain extreme configurations. It should contain a configuration very close to $(L_x, L_y) = (\sqrt{A}, \sqrt{A})$, i.e. a square box. It should also contain some configurations that are as long-and-narrow as possible. Assuming that the shortest allowed length is ℓ , these extreme long-and-narrow configurations are $(\ell, A/\ell)$ and $(A/\ell, \ell)$. Second, the total number of configurations in the set \mathcal{C} should scale as some power of A/ℓ^2 . This condition can be implemented if the lengths L_x and L_y are discretized. It should be noted that while the minimal length scale ℓ appears in several of the formulae below as a regularization parameter, the limit $\ell \rightarrow 0$ can be taken at the end without altering the conclusion of the main argument.

For the matter factors, consider $z(L_x, L_y)$ to be partition functions for a collection of N particles. Thus

$$z(L_x, L_y) = \frac{1}{N!} (z_1(L_x, L_y))^N \quad (52)$$

with

$$z_1(L_x, L_y) = \sum_{E_{L_x, L_y}} e^{-\beta E_{L_x, L_y}}. \quad (53)$$

The summation in z_1 is over the energy states available to a single particle in a box with side lengths L_x and L_y . These states may correspond to the standing waves that can form inside the two-dimensional box and, if the matter is quantum mechanical, their energies may be associated with inverse wavelengths. For nonrelativistic particles with mass m , the energy states E_{L_x, L_y} could be given by

$$E_{L_x, L_y} = \frac{1}{8m} \left(\frac{n_x^2}{L_x^2} + \frac{n_y^2}{L_y^2} \right) \quad (54)$$

with n_x and n_y the usual integer quantum numbers.

It is instructive to look at the lowest-energy particle states available in the extreme box configurations. In the large area limit these are

$$E_{min} = \begin{cases} (8m\ell^2)^{-1} & \text{for } (\ell, A/\ell) \text{ and } (A/\ell, \ell) \\ 0 & \text{for } (\sqrt{A}, \sqrt{A}). \end{cases} \quad (55)$$

The discrepancy between these two energies may be very large when ℓ is small. Minimal particle energies in nonextreme configurations lie between the two shown values.

With this particular choice of particle energy spectrum, the matter partition functions become

$$z_1(L_x, L_y) = \sum_{n_x} \exp\left(-\frac{\beta n_x^2}{8mL_x^2}\right) \sum_{n_y} \exp\left(-\frac{\beta n_y^2}{8mL_y^2}\right). \quad (56)$$

While exact expressions for (56) are not known, they can be approximated by the number of states for which β times the particle energy is less than unity¹. Such a prescription should at least provide the leading behavior of these factors. One finds

$$z_1(L_x, L_y) \sim \begin{cases} A \exp\left(\frac{-\beta}{8m\ell^2}\right) \sqrt{\frac{8m}{\beta\ell^2}} & \text{for } (\ell, A/\ell) \text{ and } (A/\ell, \ell) \\ A \frac{8m}{\beta} & \text{for } (\sqrt{A}, \sqrt{A}). \end{cases} \quad (57)$$

In the first line, it was assumed that $\beta/(8m\ell^2) > 1$.

While the leading behavior with A is the same in both cases, the contribution from the square box can be larger than those from the long-and-thin boxes when ℓ and m are small and β is large. In such cases, the dominance of the square configuration will be further amplified when $z_1(L_x, L_y)$ is raised to the power of N in (52). Of particular interest is taking N to scale with some power of A , i.e. $N \sim cA^\alpha$; the special case $\alpha = 1$ corresponds to considering a set of boxes of various areas A with fixed particle density. In the case with $N \sim A$, the matter factor $z(L_x, L_y)$ will be exponentially larger for the square configuration than for any of the other long-and-thin configurations. Moreover, since the number of nonsquare configuration scales as a power of A/ℓ^2 , the contribution of the square configuration will dominate the partition function for this toy model in the limit $A \rightarrow \infty$. Similar scaling arguments can be used to show that expectation values of observables and their fluctuations will be determined primarily by their values on the square configuration.

This example is an example of how matter degrees of freedom can determine the shape of a dynamical geometry. The result is quite striking – out of the large set of configurations \mathcal{C} , matter can select a special configuration and effectively force all observable physics to be based on this special geometry.

B. Configurations

The discussion of particles in a flexible box may be adapted to the case where the trapping container is a graph. The purpose of this section is to estimate the matter factors $z(G)$ associated with different classes of graphs in the same spirit as $z_1(L_x, L_y)$ and $z(L_x, L_y)$ were estimated above. In all cases, the number of particles, denoted N above, will be assumed to

¹ In the special case that $L_x = L_y$, z_1 may perhaps be better estimated using an integral expression

$$z_1 \sim \int_0^\infty e^{-\tilde{\beta}n^2} n \, dn$$

with $\tilde{\beta}$ being a rescaled version of β . This approach, however, does not significantly differ with the other scheme.

be the same as the number of vertices present in the graph. Thus one of the key assumptions in the following analysis is that the density of particles is constant across graphs with different number of vertices N .

1. Homogeneous Graphs

Homogeneous graphs are the easiest ones to deal with since their large-scale properties resemble lattices. Because the graphity models all have a finite number of vertices, these homogeneous lattices are closed geometries and, as discussed in Sec. IV B, represent two-dimensional tori and similar compact structures in other dimensions.

Consider first two-dimensional tori. They can be described by two lengths C_1 and C_2 representing the two circumferences. The problem of evaluating $z(G)$ for such graphs is in direct correspondence to evaluating $z(L_x, L_y)$ using (56) and (52) above. One modification that needs to be made lies in replacing the area by the number of vertices,

$$A = N\ell^2; \quad (58)$$

the factor ℓ^2 is required for dimensional reasons. Also, since each particle's wavefunction as well as its derivative should be continuous on the whole torus, the summation over particle energy states should be restricted to even integers. This restriction only rescales the estimates (57) by some factor of order one and thus the estimates made in the present case are equivalent to (57).

To obtain the full contribution of the lattice graphs to the partition function, the estimates for $z(G)$ must be combined with the nonmatter components of (38). For a torus with two circumferences almost equal, $C_1 \sim C_2 \sim \ell\sqrt{N}$, one obtains

$$\ln Z_{H, C \sim \ell\sqrt{N}}^{2d} \sim N \ln N - \beta N (g_V + \epsilon_H) + N \ln \frac{8m\ell^2}{\beta}. \quad (59)$$

For a long-and-thin torus, $C_1 \ll C_2$ or $C_2 \ll C_1$, one has

$$\ln Z_{H, C_1 \ll C_2}^{2d} \sim N \ln N - \beta N \left(g_V + a\epsilon_H + \frac{1}{8m\ell^2} \right) + \frac{1}{2} N \ln \frac{8m\ell^2}{\beta}. \quad (60)$$

In both cases, note that the factor $A^N = (N\ell^2)^N$ appearing after raising z_1 to the power of N is cancelled by the $N!$ in the denominator of (52). In the equation for the long-and-thin torus, the factor a appearing in front of ϵ_H is a real number of order one that reflects the fact that the energy per node associated with the two types of tori may be different. In particular, since the long-and-thin torus contains winding cycles that are not present in the isotropic torus [18], this factor should be expected to be greater than one.

Next, consider homogeneous graphs that represent generalizations of tori in higher dimensions d . For simplicity, consider the isotropic configurations in which all the circumferences $C \sim \ell N^{1/d}$. The generalization of (56) for this case can be written as

$$z_{1,d}(C \sim \ell N^{1/d}) = \sum_{\vec{n}} \exp \left(-\frac{\beta \vec{n}^2}{8mN^{2/d}} \right) \quad (61)$$

with \vec{n} being a d -dimensional vector of quantum numbers. Using the same approximation as before, that the sum is approximately equal to the number of states such that the exponent is less than unity, and assuming that $\beta(8m\ell^2)^{-1}N^{-2/d} < 1$, one obtains²

$$z_{1,d}(C \sim \ell N^{1/d}) \sim N \left(\frac{8m\ell^2}{\beta} \right)^{d/2}, \quad (62)$$

i.e. the same dependence on N as given by the expression (57). This is quite important: despite the number of states on a d -dimensional space up to some level $|n|$ growing as $|n|^d$, this growth is largely balanced by the smaller lengths $L \sim \ell N^{1/d}$, resulting in an overall z_1 that does not depend very strongly on d . After using this to evaluate the full contribution of the d -dimensional torus to Z_H , one therefore finds an expression that has almost the same form as (59), namely

$$\ln Z_{H,C \sim N^{1/d}}^d \sim N \ln N - \beta N (g_V + a_d \epsilon_H) + \frac{1}{2} N d \ln \frac{8m\ell^2}{\beta}. \quad (63)$$

The most important difference between this expression and (59) lies in the different energies, encoded in the real numbers a_d , associated by the graphity Hamiltonian to the different tori.

Estimating the contribution of nonisotropic d -dimensional tori to Z_H can be done in a similar fashion. As in the case of two-dimensional tori, such nonisotropic structures would contribute terms which, like (60), would contain factors $\exp(-\beta N/(8m\ell^2))$. All the different terms will not be written out here as they will turn out to not to play an important role.

2. Low-Energy Graphs

Simulations show that the lowest-energy graphs are one-dimensional chains made up of subgraphs with a small number of vertices. Since such graphs are not homogeneous lattices, one has to make further assumptions in order to guess what their matter factors should be. Suppose that these chain graphs can support particle states as standing waves both along the one-dimensional chains and also within the individual subgraphs. Then, since the substructures only have a finite number of vertices, standing waves supported within the subgraphs will have wavelengths no longer than a few ℓ . Thus, these standing waves will have a large energy; the situation is not dissimilar than for the long-and-thin boxes or tori.

This reasoning suggests to write the contribution Z_L with a factor that penalizes chain graphs for high-energy particle excitations,

$$\ln Z_L \sim N \ln N - \beta N \left(g_V + \epsilon_0 + \frac{1}{8m_L\ell^2} \right). \quad (64)$$

Here, m_L is an effective mass corresponding to the particles on the low-energy graph. It is thought to absorb all the factors that are missed in this simple estimation. What will be important is that this effective mass should not scale significantly with N and should always be positive.

² If the sum were approximated using the integral approximation in footnote 1, this would have an additional factor depending on d . This discrepancy will not be important for the argument below.

3. Random Graphs

As in the case of low-energy graphs, it is unclear how to estimate the matter factor $z(G)$ associated with random graphs. In general, the term for v_0 -random graphs can be written as

$$\ln Z_{R,v_0} \sim \frac{1}{2} N v_0 \ln N - \beta N g_V + \ln z(G_R). \quad (65)$$

Since the average distance between two vertices in a random graph is small [27], the largest wavelengths associated with particle states should be on the order of ℓ . This would suggest to write this factor similarly as in (64), for example,

$$\ln z(G_R) \sim -\frac{\beta N}{8m_R \ell^2} \quad (66)$$

with some effective positive mass m_R . Such a matter factor would be effectively penalizing random graphs for their tight connectivity.

A discussion of random nonregular graphs would follow the same lines. It will not be necessary, however, to include it here.

C. Scaling

Armed with estimates for the important components of Z , one can repeat the analysis of Sec. III B for the graphity model with matter. However, given that it was found previously that basic intuition can be extracted quite easily just by comparing the leading order behavior of the relevant terms, only this shortcut will be followed here.

Because of the additional factors due to matter, the low-energy behavior of the system can be quite different than before. Compare, for instance, the partition functions (59) and (60) associated with homogeneous graphs. The contribution due to the isotropic torus can be much larger than the contribution from long-and-thin torus if (recall that $a\epsilon_H < \epsilon_H < 0$)

$$\epsilon_H < a\epsilon_H + \frac{1}{8m\ell^2} + \frac{1}{2\beta} \ln \frac{8m\ell^2}{\beta}. \quad (67)$$

The last term on the right hand side becomes negligible if ℓ^2 is small and β large (as it is expected to be if it scales logarithmically with N). The remaining inequality may be satisfied by judiciously choosing the parameters m , ℓ , and the coupling g_B appearing inside the energy ϵ_H . Thus, matter can select the isotropic graph in the low-temperature regime even though the long-and-thin configuration contains more cycles. Next, comparing quantities (63) for various d , one can find the dimension d of the most optimal torus. This dimension d will be primarily determined by the number of short cycles, i.e. by the numbers a_d .

Suppose that the optimal dimension is $d = 2$ so that the dominant homogeneous term is given by (59). Compare this to the contribution (64) from the low-energy chainlike graphs. The homogeneous graph can be dominant if the couplings are chosen such that (recall that in general $\epsilon_0 < \epsilon_H < 0$)

$$\epsilon_H < \epsilon_0 + \frac{1}{8m_L \ell^2} + \frac{1}{\beta} \ln \frac{8m\ell^2}{\beta}. \quad (68)$$

If this is satisfied, then low-energy behavior of the graph system with matter is drastically different from what was found in Sec. III. Also, as the matter contribution to the partition function becomes important, the cycle counting becomes less so. This implies that the underlying graph structure, while preserving the large-scale properties of the emergent geometry, can perhaps become more fluid at small scales than the figures of homogeneous lattices might imply.

In the high-energy regime, just as before, random graphs can dominate above some transition temperature. The transition temperature to this regime should again be proportional to $\ln N$. The estimate of the coefficient in front of this factor should depend on the effective masses m and m_R of the particles in the high and low-temperature regimes. Since the matter factor associated with random graphs are not known in detail, this transition is not discussed further here.

VI. DISCUSSION

Summarizing, this paper focused on the classical statistical mechanics of graphity models and produced two types of results. First, results from Monte Carlo simulations show that neither $r > 0$ or $r < 0$ basic models produce ground state graphs that are latticelike. The more interesting case with negative r can at best produce an extended graph that is made up of smaller units chained together in a circle. Thus it appears that the graphity Hamiltonian that depends on vertex degrees and counts closed cycles must be supplemented with some additional conditions. Indeed, ground states searched for when the original graphity model was introduced were implicitly assumed to be homogeneous or almost homogeneous [17, 18]. Simulations of extended models implementing such homogeneity conditions in turn reveal that the intuitions in the early works [17, 18] are correct and that emergent graphs in the high inverse temperature regime can really describe extended geometries.

Second, the partition functions for the models with and without matter are estimated analytically to better understand the numerical results. In the context of the basic model without matter, such estimates, while very rough, can nonetheless provide useful information about the behavior of the graphity models in the continuum $N \rightarrow \infty$ limit. If this limit is defined through a family of models with constant couplings, the transition inverse temperature β can be shown to scale logarithmically with N . Therefore, the transition occurs at zero temperature for large N . (The transition temperature could be finite if, for example, the couplings were taken to run logarithmically with N instead.) In the context of the model including matter, estimates of the extended partition function explain how matter degrees of freedom can alter the low and high-energy behavior of a graphity model. In particular, they show that matter can enhance the importance of homogeneous graph configurations in the partition function to the extent that these graphs become dominant. Unfortunately, it was not possible to test the particular form of matter used in these estimates in numerical simulations.

The problem with nonextended configurations in the large inverse temperature regime in the graphity models is reminiscent of similar findings in the context of Euclidean dynamical triangulations [8]. In that context, the problem was noticed to become milder when the triangulation was coupled to gauge fields [21, 22], but the main solution has been based on restricting the configuration space to those triangulations respecting certain criteria motivated by causality

[8] and the presence of global spatial hypersurfaces [32]. In graphity models, such a restriction of the configurations space cannot be naturally introduced. Instead, the proposal to bypass the problem of nonextended geometries is to make the configuration space larger to include matter degrees of freedom. This is close in spirit to the mentioned work on dynamical triangulations with matter fields [21, 22]; the very interesting question of whether the mechanism described here might also regularize Euclidean dynamical triangulations deserves some further thought.

In the end, what can be learned from simple models based on graphs? At the very least, they should be seen as concrete examples of setups that do not require a continuous manifold as an ingredient but rather are able to produce one (or an approximation to one) in an appropriate regime. In particular, they can produce flat emergent geometries in the form of tori. Given this, one can start asking if some graphity model can actually reproduce the known gravitational dynamics in three plus one dimensions in some region of its parameter space, or if the discreteness may have observable consequences for particle physics or cosmology (works studying related issues in similar models include [33, 34].) These are issues that are worth exploring further and now bring graphity models, which begin at a slightly speculative starting point, possibly close to being compared with experiment.

Acknowledgments. I would like to thank my colleagues for discussions and comments on the manuscript. I am very grateful to G. Barkema, in particular, for practical programming tips leading to speeding up cycle counting and for advice regarding Monte Carlo simulations in general.

-
- [1] D. Oriti, “Group field theory as the microscopic description of the quantum spacetime fluid: a new perspective on the continuum in quantum gravity,” arXiv:0710.3276 [gr-qc].
 - [2] J. C. Baez, “An introduction to spin foam models of BF theory and quantum gravity,” Lect. Notes Phys. **543**, 25 (2000) [arXiv:gr-qc/9905087].
 - [3] A. N. Jourjine, “Dimensional Phase Transitions Coupling Of The Matter To The Cell Complex,” Phys. Rev. D **31**, 1443 (1985).
 - [4] J. Henson, “The causal set approach to quantum gravity,” arXiv:gr-qc/0601121.
 - [5] D. P. Rideout and R. D. Sorkin, Phys. Rev. D **61**, 024002 (2000) [arXiv:gr-qc/9904062].
 - [6] M. Requardt, “(Quantum) space-time as a statistical geometry of lumps in random networks,” Class. Quant. Grav. **17**, 2029 (2000) [arXiv:gr-qc/9912059].
 - [7] F. Markopoulou, “Quantum causal histories,” Class. Quant. Grav. **17**, 2059 (2000) [arXiv:hep-th/9904009].
 - [8] J. Ambjorn, J. Jurkiewicz and R. Loll, “Dynamically triangulating Lorentzian quantum gravity,” Nucl. Phys. B **610**, 347 (2001) [arXiv:hep-th/0105267].
 - [9] J. Ambjorn, J. Jurkiewicz and R. Loll, “Reconstructing the universe,” Phys. Rev. D **72**, 064014 (2005) [arXiv:hep-th/0505154].
 - [10] J. Ambjorn, J. Jurkiewicz and R. Loll, “Emergence of a 4D world from causal quantum gravity,” Phys. Rev. Lett. **93**, 131301 (2004) [arXiv:hep-th/0404156].
 - [11] C. Rovelli, *Quantum Gravity*, Cambridge University Press, New York (2004).

- [12] T. Thiemann, “Introduction to modern canonical quantum general relativity,” arXiv:gr-qc/0110034.
- [13] K. Giesel and T. Thiemann, “Algebraic quantum gravity (AQG). I: Conceptual setup,” *Class. Quant. Grav.* **24**, 2465 (2007) [arXiv:gr-qc/0607099].
- [14] C. Barcelo, S. Liberati and M. Visser, “Analogue gravity,” *Living Rev. Rel.* **8**, 12 (2005) [arXiv:gr-qc/0505065].
- [15] G. E. Volovik, “Fermi-point scenario for emergent gravity,” arXiv:0709.1258 [gr-qc].
- [16] O. Dreyer, “Emergent general relativity,” arXiv:gr-qc/0604075.
- [17] T. Konopka, F. Markopoulou and L. Smolin, “Quantum Graphity,” arXiv:hep-th/0611197.
- [18] T. Konopka, F. Markopoulou and S. Severini, “Quantum Graphity: a model of emergent locality,” arXiv:0801.0861 [hep-th].
- [19] F. Markopoulou, “Towards gravity from the quantum,” arXiv:hep-th/0604120.
- [20] S. Kalyana Rama, “A principle to determine the number (3+1) of large spacetime dimensions,” *Phys. Lett. B* **645**, 365 (2007) [arXiv:hep-th/0610071].
- [21] S. Bilke, Z. Burda, A. Krzywicki, B. Petersson, J. Tabaczek and G. Thorleifsson, “4d simplicial quantum gravity interacting with gauge matter fields,” *Phys. Lett. B* **418**, 266 (1998) [arXiv:hep-lat/9710077].
- [22] S. Bilke, Z. Burda, A. Krzywicki, B. Petersson, J. Tabaczek and G. Thorleifsson, “4d simplicial quantum gravity: Matter fields and the corresponding effective action,” *Phys. Lett. B* **432**, 279 (1998) [arXiv:hep-lat/9804011].
- [23] M. Levin and X. G. Wen, “Fermions, strings, and gauge fields in lattice spin models,” *Phys. Rev. B* **67**, 245316 (2003) [arXiv:cond-mat/0302460]
- [24] M. A. Levin and X. G. Wen, “String-net condensation: A physical mechanism for topological phases,” *Phys. Rev. B* **71**, 045110 (2005) [arXiv:cond-mat/0404617]
- [25] M. Levin and X. G. Wen, “Quantum ether: Photons and electrons from a rotor model,” arXiv:hep-th/0507118.
- [26] J. B. Kogut and L. Susskind, “Hamiltonian Formulation Of Wilson’s Lattice Gauge Theories,” *Phys. Rev. D* **11**, 395 (1975).
- [27] N. Wormald, “Models of random regular graphs,” *Surveys in Combinatorics, 1999 (Canterbury)*, (J. D. Lamb and D. A. Preece, eds.), pp. 239-298, London Math. Soc. Lecture Note Ser., 267, Cambridge Univ. Press, Cambridge, 1999.
- [28] M. E. J. Newman and G. T. Barkema, *Monte Carlo Methods in Statistical Physics*, Oxford University Press, 2002.
- [29] Simulations are performed with a custom program called Graphity Monte Carlo. The java source code as well as compiled class files can be found in the source package associated with this paper on the arXiv.
- [30] A. Steger, and N. C. Wormald, “Generating random regular graphs quickly,” *Combinatorics, Probability and Computing* **8** (1999), 377-396.
- [31] N. Schupper and N. M. Shnerb, “Inverse melting and inverse freezing: A spin model,” *Phys. Rev. E* **72**, 046107 (2005) [cond-mat/0502033v1]
- [32] T. Konopka, “Foliations and 2+1 causal dynamical triangulation models,” *Phys. Rev. D* **73**, 024023 (2006) [arXiv:hep-th/0505004].
- [33] F. Dowker, J. Henson and R. D. Sorkin, “Quantum gravity phenomenology, Lorentz invariance

- and discreteness,” *Mod. Phys. Lett. A* **19**, 1829 (2004) [arXiv:gr-qc/0311055].
- [34] J. Magueijo and P. Singh, “Thermal fluctuations in loop cosmology,” *Phys. Rev. D* **76**, 023510 (2007) [arXiv:astro-ph/0703566].

